Influence of nitrogen doping on the radial breathing mode in carbon nanotubes

Iann C. Gerber,[1,*] Pascal Puech,[2] Anis Gannouni,[1,†] and Wolfgang Bacsa[2]
[1]*INSA, UPS, CNRS, Université de Toulouse, LPCNO 135 Avenue de Rangueil, F-31077 Toulouse, France*
[2]*UPS, CNRS, Université de Toulouse, CEMES 29 rue Jeanne Marvig, F-31055 Toulouse, France*
(Received 2 October 2008; revised manuscript received 12 December 2008; published 11 February 2009)

The influence of nitrogen doping in semiconducting carbon nanotubes is investigated by first-principles calculations considering a wide variety of substitution sites and concentrations. The frequency of the radial breathing mode of a (8,0) nanotube is calculated using density-functional theory and frozen-phonon approximation for different doping concentrations, substitution sites, and vacancies. The results are compared to a one-dimensional first-neighbor spring constant model using experimental parameters. We estimate the effect of doping in Raman spectra by examining the electronic band structure of doped carbon nanotubes.

DOI: 10.1103/PhysRevB.79.075423 PACS number(s): 81.07.De, 82.20.Wt, 63.22.−m, 78.30.Na

I. INTRODUCTION

Carbon nanotube (CNT) properties are directly related to their particular structure. Most growth processes of carbon nanotubes (see Ref. 1 for a review) lead to a relatively wide distribution in diameter and length. Recent studies have shown how the diameter distribution can be narrowed or how CNTs can be sorted according to their helicity or chirality.[2] Doping CNTs is an attractive alternative to control the electronic conductivity of CNTs independently of their diameter.[3–6] Highly conducting nanotubes are of interest for applications in transparent thin-film electrodes and other applications.

In a simple picture, doping CNTs through substitution of a single carbon atom by a nitrogen atom results in one additional electron in the π-electron system. This additional electron depending of the CNT band structure[7] can induce significant modifications of the density of states (DOS) in the vicinity of the Fermi level.[4] For instance when the extra electron is localized in semiconducting CNTs, the corresponding dopant state is a quasibound state. This quasibound state can be considered as the one-dimensional (1D) analog of *n*-type donors in semiconductors.[5]

Raman spectroscopy is one of the most frequently used noninvasive diagnostic tool for CNTs.[8] Resonant excitations make the method highly sensitive to individual tubes, and as a result spectral mapping gives direct access to heterogeneity and size distribution, important for the development of efficient synthesis processes. One of the important information available from Raman spectra of CNTs is the spectral band due to the radial breathing mode (RBM). The RBM corresponds to an in-phase motion of the atoms in radial direction. Its frequency is inversely proportional to the tube diameter (d),

$$\omega_{\mathrm{RBM}} = \frac{C_1}{d} + C_2, \tag{1}$$

C_2 is added to account for the interaction with the surrounding.[9] Due to the inverse relationship between frequency and diameter, the nanotubes need to have a diameter smaller than 10 Å to assign RBM bands to a particular chirality (helicity) of single wall carbon nanotube (SWNTs) (Refs. 10–15) without ambiguity.

Experimentally, vibrational spectra from carbon nitride films[16] show two dominant bands corresponding to the C-N vibrations and two bands related to C-C vibrations. The bands at 1100 and 1470 cm^{-1} have been attributed to C-N stretching modes by analogy with molecules containing fairly symmetric tetrahedral carbon-nitrogen bonds (N-N stretching mode in C-N-N-C configuration). The bands at 1350 and 1581 cm^{-1} are characteristic for sp^2 bonded carbon. Nitrogen doping in SWNTs is expected to modify the RBM frequency depending on concentration and the substitution site of the dopant.

The energy of the RBM on undoped tubes has been studied in detail experimentally and theoretically by means of zone folding schemes,[9] spring constant models,[17] and first-principles calculations.[10,18,19] Several important advances in carbon nanotube research such as sorting tubes[20] or the determination of transition energies of individual CNTs (Ref. 12) are directly related to the observation of RBMs. The influence of doping on RBMs have been examined using silver (*n* doping)[21] or applying electrical potentials in electrochemical cells.[22] We considered here in detail the influence of substitution site and concentration on the RBM frequency when doping CNT with nitrogen.

We first describe computational details (Sec. II) about the relaxation of the tube structure and the calculation of the RBM frequencies. We then present the results concerning the density-functional theory (DFT) calculations of N-substituted (8,0) CNTs and discuss geometrical similarities with previous studies (Sec. IV). We compare the results of the RBM frequency of doped (8,0) CNTs at various substitution configurations with a one-dimensional first-neighbor spring constant model in Sec. III. At the end, we discuss the influence of nitrogen doping in Raman spectra of CNTs.

II. COMPUTATIONAL DETAILS

To determine the RBM shift with N doping, we have carried out DFT calculations using the Vienna *ab initio* simulation package (VASP).[23,24] The code uses the full-potential projector augmented wave (PAW) framework.[25,26] Exchange-correlation effects have been approximated using the PBE (Ref. 27) functional and applied in spin-polarized calculations. A kinetic-energy cutoff of 400 eV was found to be

sufficient to achieve a total-energy convergence within several meV considering k-point sampling. All atoms were fully relaxed to forces on individual atoms smaller than 0.02 eV/Å.

We selected (8,0) zigzag CNTs for the model calculations and considered two primitive unit cells containing together 64 atoms. The tube is oriented along the z axis and placed in a unit cell sufficiently large in the two perpendicular directions (16×16 Å^2) to reduce interactions to a threshold of less than 1 meV/atom for the cohesive energy. A carbon covalent bond length of 1.42 Å has been chosen as a starting value before optimization. The doping concentration was controlled by the substitution of one to three carbon atoms with nitrogen atoms resulting in a maximum doping concentration of 5%.

We have applied the frozen-phonon approximation as described in Ref. 10 to calculate the RBM mode with and without doping in the (8,0) CNTs by means of fitting the total energy for several atomic positions. These configurations were obtained by moving uniformly every atoms of the unit cell in radial direction out of the equilibrium position by $\pm 1\%$ and $\pm 2\%$, giving access to the harmonic force constants and the RBM frequency. To compare with the results of first-principles calculations, we use a one-dimensional spring constant model which takes into account nitrogen substitution by scaling of the pristine RBM frequency.

III. ONE-DIMENSIONAL SPRING CONSTANT MODEL

A. Spring constant model

To calculate the frequency of a RBM with a force-constant model, we need to define and diagonalize the corresponding dynamical matrix. For CNTs at least two force constants are required, bond length changes and bond bending (k_r, k_θ). Introduction of a dopant leads to two additional force constants. In the case of armchair tubes, we find that there is a direct correlation between the eigenvector of the mode corresponding to the RBM and the G bands. For the vibrational mode corresponding to the G band, neighboring atoms are displaced out of phase (antisymmetric) while for the RBM the neighboring atoms are displaced in phase (symmetric). The similarity of the displacement pattern for the two modes leads to a fundamental relation of their energies. To reduce the number of parameters we consider here only a one-dimensional spring constant model. We use the frequency of the G band as the only input parameter and show below that the effect of doping can be included by scaling.

B. Pristine CNTs

When considering Newton's equation for a linear chain of atoms (spring constant k) and considering the vibrational mode of the G band which corresponds to an out of phase stretching motion of neighboring atoms with mass m_C, we can write for the frequency,

$$\omega_{\mathrm{G}}^2 = \frac{4k}{m_C}. \tag{2}$$

Considering a closed linear chain in circumferential direction we have

TABLE I. Summary of the experimentally determined constants C_1 and C_2 of Eq. (1).

C_1	C_2	Ref.
226	12.5	12
215	18	14 and 28
223[a], 218[b]	10[a], 18[b]	29
207	27	30

[a]Metallic tubes.
[b]Semiconductor tubes.

$$\frac{1}{K_{\mathrm{tube}}} = \sum_i \frac{1}{k} \Rightarrow K_{\mathrm{tube}} = \frac{ka}{\pi d}, \tag{3}$$

where a is the bond length and d the diameter. The mass for a closed chain or tube section is

$$M_{\mathrm{tube}} = m_C \frac{\pi d}{a}. \tag{4}$$

The Lagrangian $\mathcal{L}$ for a tube section is

$$\mathcal{L} = \frac{1}{2} M_{\mathrm{tube}} \dot{r}^2 - \frac{1}{2} K_{\mathrm{tube}} \Delta l^2, \tag{5}$$

where $\dot{r}$ is the speed in radial direction and Δl is the change in the length of circumference. We can rewrite this expression as,

$$\mathcal{L} = \frac{1}{2} M_{\mathrm{tube}} \dot{r}^2 - \frac{1}{2} K_{\mathrm{tube}} (2\pi \Delta r)^2, \tag{6}$$

$$\mathcal{L} = \frac{1}{2} M_{\mathrm{tube}} \dot{r}^2 - \frac{1}{2} K_{\mathrm{tube}}^{\mathrm{radial}} (\Delta r)^2 \tag{7}$$

when introducing a spring constant along the radial direction. Using the Euler-Lagrange equation, we obtain

$$\omega_{\mathrm{RBM}}^2 = \frac{K_{\mathrm{tube}}^{\mathrm{radial}}}{M_{\mathrm{tube}}} = 4\pi^2 \frac{ka}{\pi d} \frac{a}{m_C \pi d} = \omega_{\mathrm{G}}^2 \frac{a^2}{d^2}. \tag{8}$$

With $\omega_{\mathrm{G}} = 1581$ cm^{-1} and $a = 1.42$ Å, the RBM is given by

$$\omega_{\mathrm{RBM}} \ (\mathrm{cm}^{-1}) = \omega_{\mathrm{G}} \frac{a}{d} = \frac{225}{d} \ (\mathrm{nm}^{-1}). \tag{9}$$

This shows that the frequency of the RBM ω_{RBM} is directly related to the frequency of the G band ω_{G}. By neglecting the influence of chirality on the RBM frequency we obtain for a (8,0) pristine nanotube using Eq. (9): $\omega_{\mathrm{RBM}}^{\mathrm{prist}}(8,0) = 358.5$ cm^{-1}.

The RBM frequency in function of diameter [Eq. (1)] has been explored experimentally by several groups. Table I shows experimentally determined values for C_1 and C_2.

The C_1, as determined by the one-dimensional spring constant model for armchair tubes using the frequency of the Raman G band and C-C bond length, is very close to the experimentally found value of C_1. C_2 has been originally added to account for the interaction of the tube with the environment which is related to charge transfer or changes in

the electron-phonon coupling. These effects are not included in the linear-chain model.

C. Influence of N doping on RBM in CNTs

We modify the previous expressions for the frequency of the RBMs of pristine tubes to include changes induced by nitrogen doping. Substitution has the effect of changing the mass and the spring constant. We assume no modification of bond length in first approximation.

By defining the atomic fraction of nitrogen as $x=n_N/(n_N+n_C)$ and by taking the double of a primitive unit cell of a (8,0) tube (64 atoms) with 96 bonds, a single substitution modifies three bonds which yields an atomic fraction of nitrogen of $3/96=2/64=2x$. We can then replace the energy of the optical phonon in Eq. (9) ω_G by an effective phonon energy ω^{eff}. It has been reported that nitrogen substitution in carbon[16] leads to a localized C-N vibrational mode ($\omega_{\text{C-N}}$) in tetrahedral configuration at 1100 cm^{-1}. We can scale the energy of the localized vibrational mode by the fraction of the number of C-C bonds which have been replaced by C-N bonds. We find after substitution in Eq. (9) with the corresponding definition of the effective phonon energy, $\omega^{\text{eff}}=(1-2x)\omega_G+2x\omega_{\text{C-N}}$:

$$\omega_{\text{RBM}}^{\text{doped}}(x) = \omega_{\text{RBM}}\left(1 - 2x\frac{\omega_G - \omega_{\text{C-N}}}{\omega_G}\right) \tag{10}$$

$$\approx \omega_{\text{RBM}}^{\text{prist}}(1 - 0.6x), \tag{11}$$

where $\omega_{\text{RBM}}^{\text{prist}}$ corresponds to the pristine tube frequency defined by Eq. (9). By including the effect of mass and spring constant, we can estimate doping effects as a function of concentration for SWNTs.

We can treat the case for two adjacent dopants by taking into account five modified bounds. With $x=2/64=1/32$ and considering that four C-N and one N-N bond are formed, the effective phonon energy is $\omega^{\text{eff}}=(1-5/96)\omega_G+4/96\omega_{\text{C-N}}+1/96\omega_{\text{N-N}}$ which yields a downshift of -4.8 cm^{-1} for the RBM frequency which is slightly larger than in the single substitution case (-3.4 cm^{-1}).

Vacancies have been observed experimentally.[31] We can consider vacancies by removing a single carbon atom and associating three bonds to zero frequency in the effective phonon energy by removing three C-C bonds, $\omega^{\text{eff}}=(1-3/96)\omega_G$. This yields a downshift of -11.2 cm^{-1} for a single vacancy. We can also calculate the effect of a pyridinelike structure[5] in doped CNTs by substituting carbon atoms by three nitrogen atoms with a neighboring vacancy site (see Fig. 3). The effective phonon energy arising for this configuration can be estimated by removing nine C-C bonds and adding only six C-N bonds. We exclude N-N bonds between the three nitrogen atoms because the distances are too large, and we obtain $\omega^{\text{eff}}=(1-9/96)\omega_G+6/96\omega_{\text{C-N}}$ corresponding to a downshift of -18.0 cm^{-1} for a (8,0) tube.

IV. RESULTS OF DFT CALCULATIONS

Doping concentrations of nitrogen in SWNTs in the literature are found to be low so far and lie in the few percent range.[32,33] We have thus considered two primitive unit cells containing 64 carbon atoms of a (8,0) tube with a single (Fig. 1) and several double substitution configurations. The different double substitution configurations are summarized in Fig. 2. The vacancy and pyridinelike structure are shown in Fig. 3. We first discuss the structural constraints and the energy stability. We then present our results on the RBM frequencies and compare them to the one-dimensional spring constant model. We finally discuss the electronic band structure of doped CNTs.

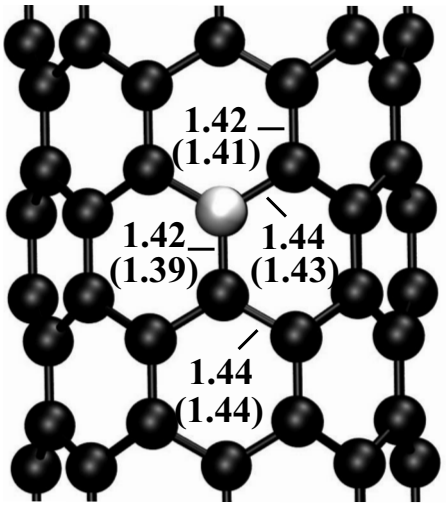

FIG. 1. Relaxed geometry of a single nitrogen substitution in a (8,0) tube. Bond lengths before and after substitution (in parenthesis) are given in Å.

A. N-induced structural modifications

First studies[34–37] of nitrogen doped CNTs have appeared recently. It has been stated that deformations induced by substitution are small and not much attention has been given so far to structural modifications of the tube wall induced by doping.[3] We show here that structural modifications induced by doping can have a sizeable effect on the RBM frequency.

We start with a pristine nanotube with a fixed carbon bond length of 1.42 Å. Energy optimization leads to an increase in the bond length of less than 1% for circumferential bonds ($d_{\text{C-C}}^{zz}$) and a reduction in the bond length of up to 0.2% for bonds along the tube axis ($d_{\text{C-C}}^{\text{axis}}$); see Fig. 1. This difference along the two main directions of the tube is confirmed by changing the size of unit cell. The same bond lengths have been obtained with eight primitive unit cells. We assume that the bond length changes are induced by the tube curvature.

When substituting one carbon atom, the nearest neighbors are the most affected, leading to C-N bond lengths smaller the C-C bond length. Modifications in the second-nearest-neighbor positions are small while bonds along tube axis ($d_{\text{C-C}}^{\text{axis}}$) are reduced by 2% whereas bonds in circumferential direction stay identical. We observe no change in the pyramidal angle. The pyramidal angle is a measure of the angle between the σ and π orbitals,[38] $\Theta_p=10.2°$. This means that the nitrogen atom does not project out of the tube wall. This absence of any radial displacement is also reflected in the

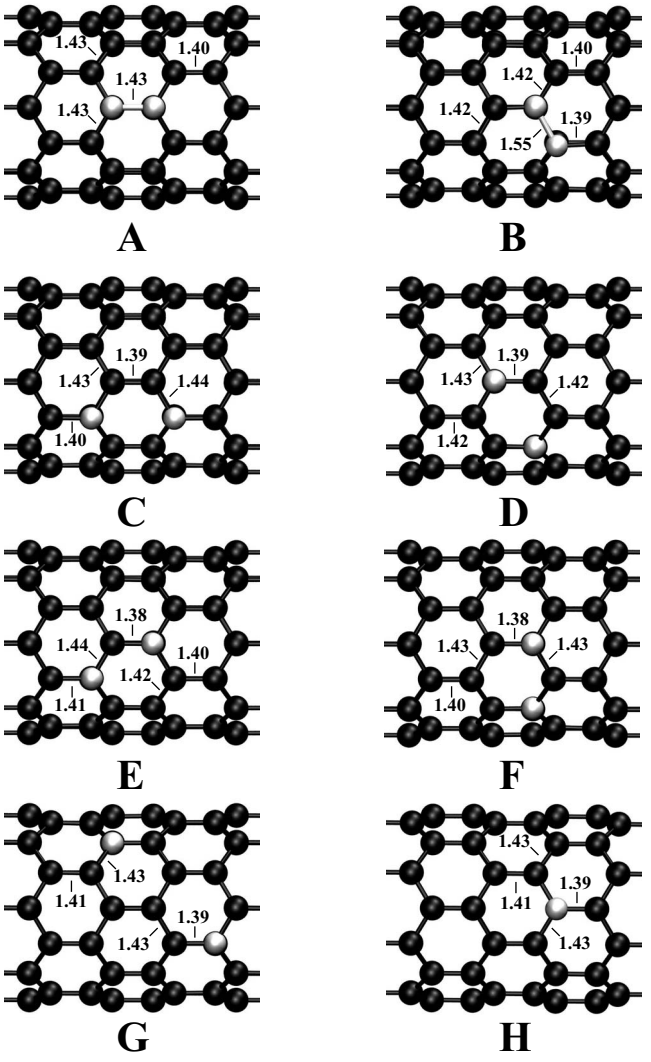

FIG. 2. Relaxed geometries containing two substitutions (C atoms in black, N atoms in white). The **H** configuration corresponds to two N atoms in diametrical opposite positions. Bond lengths are given in Å.

deformation parameter, defined as $\delta = d_{\min}/d_{\max}$; for pristine tubes $\delta = 1.0$.

With a second substituted carbon atom within the unit cell we need to consider several substitution configurations. The bond lengths of the optimized structure, pyramidal angle, and deformation parameter of all considered configurations are shown in Table II. The substitution configurations can be grouped in two subgroups: two directly bound nitrogen atoms (in Fig. 2, configurations **A** and **B**) and two well-separated nitrogen atoms (in Fig. 2, from **C** to **H** configurations). In all the considered cases, the modifications of the second-nearest-neighbor positions are small, with reductions in C-C bond lengths along the tube axis and an increase in $d^{zz}_{\text{C-C}}$; see Table II. The C-N bonds along the tube axis are smaller than the C-C bonds while $d^{zz}_{\text{C-N}}$ are systematically longer than 1.42 Å.

In the cases **A** and **B** with two associated nitrogen atoms, there is a relative large distortion of the diameter $\delta = 0.94$ and $\delta = 0.91$, respectively. The pyramidal angle Θ_p is also larger

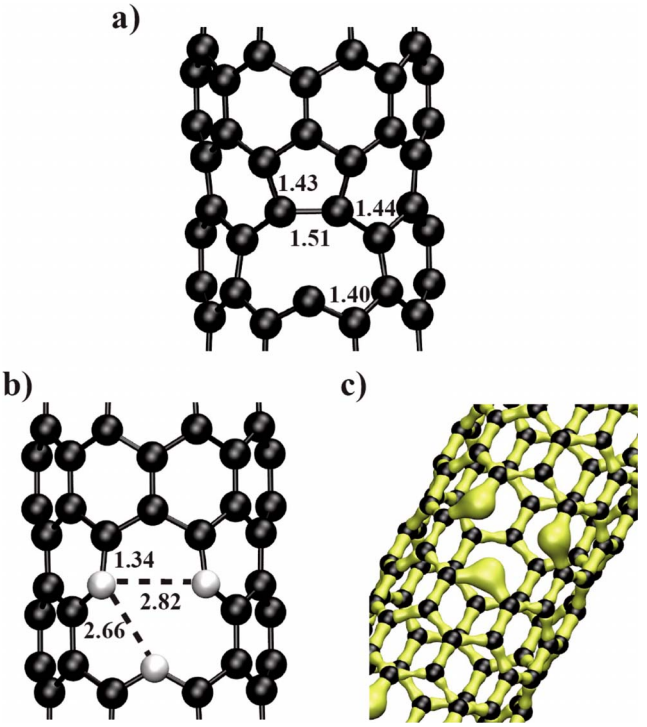

FIG. 3. (Color online) Relaxed geometry of a single vacancy (a) and a pyridinelike configuration (b) in the (8,0) CNT. (c) Total valence density snapshot of the pyridinelike structure with a cutoff value of $1.8e/\text{Å}^3$. Carbon atoms are indicated in black and nitrogen atoms in white.

compared to the case with a single substitution. This shows that the nitrogen atoms tend to repel each other by increasing their displacement in the radial direction. All others configurations with two nitrogen atoms show only minor changes compared to the configuration with one nitrogen atom.

Vacancies in SWNTs have been studied previously,[39–42] and it is known that structural reorganization can take place with the creation of a pentagon leading to a single dangling bond. The optimized geometry of the (8,0) tube with a vacancy is shown in Fig. 3(a). The basal C-C bond length of the pentagon ring is 1.51 Å, longer than the normal sp^2 bond length. The carbon atom with the dangling bond is displaced in radial direction.

Detailed analysis of the N-π edge by HREELS,[43] as well as x-ray photoelectron spectroscopy and electron-tunneling spectra,[5] shows the formation of pyridinelike configurations which are energetically stable in nitrogen rich nanotubes. Figure 3(b) displays the optimized structure of a pyridinelike structure in a (8,0) tube. The C-N bonds are characteristic for pyridine with a bond length of 1.34 Å. We observe again a repulsion of two neighboring nitrogen atoms due to tube curvature. The two nitrogen atoms are separated by a minimum distance $d_{\text{N-N}} = 2.66$ Å indicating that no covalent bond is formed between them. This is confirmed by a detailed analysis of the charge density, where lone pairs of nitrogen atoms can be seen in Fig. 3(c).

B. Formation energy

The formation energy of SWNT's doped with nitrogen (E_f^{dop}) can be written in terms of the cohesive energy per

TABLE II. C-N and C-C bond lengths in Å for first- and second-nearest neighbors, pyramidal angle Θ_p in different substitution configurations, as reported in Fig. 2. The values of the **G** and **H** configurations are not shown since they correspond to the single substitution case.

Substitution mode	$d_{\text{N-N}}$	$d^{\text{axis}}_{\text{C-N}}$	$d^{zz}_{\text{C-N}}$	$d^{\text{axis}}_{\text{C-C}}$	$d^{zz}_{\text{C-C}}$	Θ_p (deg)	δ
A	1.43		1.43	1.40	1.43	15.1	0.94
B	1.55	1.39	1.42	1.40	1.42	18.8/10.1	0.91
C		1.40	1.44	1.39	1.43	13.8	0.96
D		1.39	1.43/1.44	1.42	1.42/1.43	11.7/10.8	0.99
E		1.38/1.41	1.44	1.40	1.42/1.43/1.44	13/8.8	0.96
F		1.38	1.43	1.40	1.43/1.44	11.0/8.7	0.99

atom of the pristine tube E_c^{prist} containing l carbon atoms. The cohesive energy per atom of doped tubes with k nitrogen atoms ($E_c^{k\text{N}}$) is

$$E_c^{\text{prist}} = \frac{E_t^{\text{prist}} - lE_{\text{C}}}{l}, \tag{12}$$

$$E_c^{k\text{N}} = \frac{E_t^{\text{dop}} - kE_{\text{N}} - (l-k)E_{\text{C}}}{l}, \tag{13}$$

$$E_f^{\text{dop}} = l(E_c^{k\text{N}} - E_c^{\text{prist}}), \tag{14}$$

where E_t^{prist}, E_t^{dop}, E_{C}, and E_{N} denotes the total energy of the pristine tube, the total energy of a doped tube, and the energy of a single carbon and nitrogen atoms, respectively. We use $E_{\text{C}}=E_t^{\text{prist}}/l$ as the reference energy of a carbon atom, and $E_{\text{N}}=1/2E_t(\text{N}_2)$ for a nitrogen atom. To compare the formation energy from different nanotubes as a function of concentration, we can define a formation energy per substituted atom,

$$E_f^{k\text{N}} = \frac{(E_t^{\text{dop}} + kE_{\text{C}}) - (E_t^{\text{prist}} + kE_{\text{N}})}{k}. \tag{15}$$

Figure 4 shows the formation energy for all configurations containing two nitrogen atoms. We find that configurations

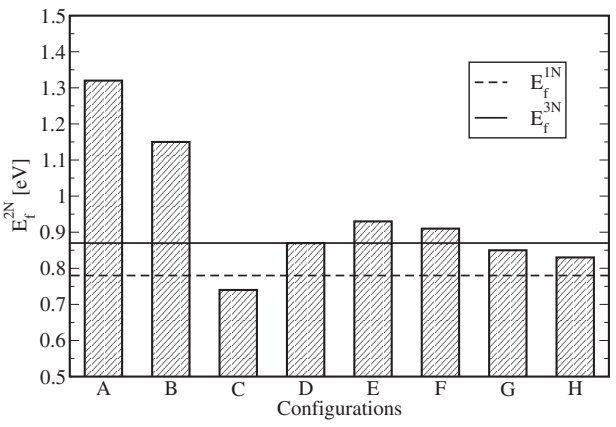

FIG. 4. Formation energies E_f of isomers as presented in Fig. 2. $E_f^{1\text{N}}$ is the formation energy of a single substitution while $E_f^{3\text{N}}$ is the formation energy of a triple substitution.

with two associated nitrogen atoms are less stable which is coherent with what has been previously reported.[34,36,37,44] The largest energy difference between the most stable (**C**) and the less stable (**A**) configuration is 0.58 eV per nitrogen atom which compares relatively well with the differences of 0.46 (Ref. 34) and 0.77 eV (Ref. 36) per nitrogen atom for a (10,0) tube, but is only half of the value published recently for the (8,0) tube using cluster model calculation.[37] This difference can be attributed to the cluster model calculation in which tubes are modeled with open ends terminated with hydrogen atoms.[37] Cluster model calculations tend to overestimate substitution energies, especially when a relatively small tube section is used. From the difference in the formation energies we see that there is a driving force that ensures that the nitrogen atoms are not neighbors. We find that the most stable configuration is not the **H** configuration where the nitrogen atoms are diametrically opposed, but the **C** configuration. The formation energy of configuration **C** is even smaller than a single substitution by 40 meV per nitrogen atom. This indicates that the correlation between two additional electrons tends to improve the stability.

The high formation energy of the **A** and **B** configurations can be explained by the energy cost to bind two nitrogen atoms. We observe in configuration **A** ($d_{\text{N-N}}=1.44$ Å) and **B** ($d_{\text{N-N}}=1.55$ Å) that the influence of the sp^2 bonding in its neighborhood is important. The structure of the tube wall keeps the nitrogen atoms bound to three neighbors. This effect is more pronounced in the **A** configuration where the N-N bond direction is axial, while in **B** case, nitrogen atoms can move slightly in radial direction decreasing the cohesive energy. The same effect has been observed in the case of (10,0) tubes with an energy difference between the two configurations of 0.11 eV/atom (Ref. 34) and 0.31 eV/atom.[36] This is clearly different from armchair tubes where it has been shown that nitrogen atoms can be first nearest neighbors associated with structural adjustments without increasing the formation energy considerably.[34]

Using the following definition of the formation energy of the vacancy: $E_f^{\text{vac}}=E_t^{\text{def}}-(l-1)E_t^{\text{prist}}/l$, where E_t^{def} is the total energy of the defective tube, we find 5.32 eV for the (8,0) tube. This compares well with previous published estimations of 4.8 (Ref. 41) and 5.5 eV (Ref. 42) but is relatively high compared to the energy of a single substitution. The total formation energy for a vacancy can be lowered considerably by adding three successive substitutions to form a

pyridinelike structure [Fig. 3(b)]. In this case the substitution energy per nitrogen atom decreases by 0.99 eV which yields a value which is close to the substitution energy in pristine tube. This suggests that the formation of pyridinelike structures can be induced in a nitrogen rich atmosphere.

Our calculations show that nitrogen substitution induces structural changes and increases the formation energy. We use in the following the frozen-phonon approach to evaluate the RBM frequency as a function of doping.

C. RBM frequencies of N-doped CNTs

RBM frequencies in pristine CNTs have been previously calculated using zone folding,[9,45–48] classical mechanics,[17] and first-principles calculations.[10,18,19,49] The effect of curvature and chirality on the phonon spectrum has been investigated analytically.[50–52]

RBM Raman bands are resonantly enhanced when the incident or the scattered photon coincide with one of the singularities in the joined density of states.[8] The resonance profile for RBMs is typically 50–80 meV wide for individual SWNTs. The formation of excitons in CNTs has the effect to lower the transition energies and modifies the tube structure at the location of the exciton. Excitonic effects are not taken into account in our frozen-phonon approach.

Considering the (8,0) pristine nanotube, and only taking into account radial components,[18,48] we obtain from our PBE-based calculations, a RBM frequency of 357.3 cm^{-1}. This value agrees within 13 wave numbers with results of Refs. 18 and 19, 363.6 and 370 cm^{-1}, respectively. The difference with the value of Kürti *et al.*[18] is believed to be due to the level of approximation used in the calculation. We use here a more accurate approximation of the exchange-correlation functional compared to earlier reports. It is known that LDA tends to overbind carbon atoms which results in a contraction of the tube diameter and a large value of the force constants. As a result, LDA calculations overestimate RBM frequencies. Using the PBE functional we obtain smaller force constants and smaller tube diameters resulting in smaller RBM frequencies. The agreement between the DFT calculations and the one-dimensional spring constant model is within 1.2 cm^{-1} corresponding to an error of less than 1%.

DFT calculations predict a downshift of −5.8 cm^{-1} while the one-dimensional spring constant model predicts a downshift of −3.4 cm^{-1} for 3.1% nitrogen doping. The effect of the additional electron is to downshift or soften the phonon. This is consistent with results on Li-doped CNTs (Ref. 53) and the study of oxygen-functionalized CNTs.[54]

As the doping concentration increases one has to take into account the possible formation of N-N bonds. For the **A** and **B** configurations (Fig. 2) the one-dimensional spring constant model gives −4.8 cm^{-1}, which is smaller than DFT calculation, −9.1 cm^{-1} (Table III). A second additional electron leads to larger structural modifications and a larger downshift of the RBM band. For the other configurations, i.e., from **C** to **H**, the downshift are smaller, ranging from −2.9 to −7.2 cm^{-1} using the DFT calculations.

The simple one-dimensional spring constant model cannot discriminate between the different dopant sites and gives the same downshift of −6.7 cm^{-1} for all substitution configurations. The one-dimensional spring constant model neglects completely the local distortion induced by the nitrogen atom as well as the correlation effects of the two extra electrons in the unit cell considered in the calculation. The largest difference between the two methods occurs for the H configuration. The small downshift in the highly symmetric configuration is unexpected. This points to the fact that the symmetry of the dopant sites is important for the RBM frequency. In summary, nitrogen substitution leads to a downshift of −2.9 to −9.1 cm^{-1} depending on substitution configuration and softening of the chemical bonds.

TABLE III. RBM frequency of pristine (8,0) nanotube and nitrogen substitution induced downshifts as determined by DFT calculations and one-dimensional spring constant model in cm^{-1}.

	DFT	SC model	Downshift
Pristine	357.3	358.5	
1-N	351.5	351.8	−5.8/−3.4
A	348.2	353.8	−9.1/−4.8
B	349.3	353.8	−8.0/−4.8
C	352.5	351.8	−4.8/−6.7
D	351.4	351.8	−5.9/−6.7
E	352.0	351.8	−5.3/−6.7
F	350.1	351.8	−7.2/−6.7
G	350.6	351.8	−6.7/−6.7
H	354.4	351.8	−2.9/−6.7
Vacancy	348.8	347.3	−8.5/−11.2
Pyridinelike	352.8	340.5	−4.6/−18.0

Defects in the walls of CNTs have been experimentally observed. Defects are believed to play an important role in the structural dynamics of CNTs. Clearly, local structural disturbances influence RBM frequencies. We find for a single vacancy that the RBM frequency is downshifted by −8.5 cm^{-1} using DFT which agrees well with a recent study of the characteristic vibrational modes of a single vacancy in a zigzag tube.[55] The one-dimensional spring constant model gives a larger downshift of −11.2 cm^{-1}. Vacancies and pyridinelike structures lead to structural modifications and changes in hybridization which are not taken into account in the one-dimensional spring constant model but are included in the DFT calculations. We conclude that vacancies, pyridinelike structures in the tube wall, and nitrogen doping induces downshifts of the same order of magnitude.

D. Electronic band structure

Figure 5 shows the calculated electronic band structure for CNTs with one and two substitutions (in configuration **C**) demonstrating a upshift of the Fermi level in doped nanotubes. The allowed optical transitions for pristine tube are indicated following the interpretation of Spataru *et al.*,[56] neglecting many-body effects. Our DFT calculations compare well with recently published work[21] of the electronic band structure of CNTs.

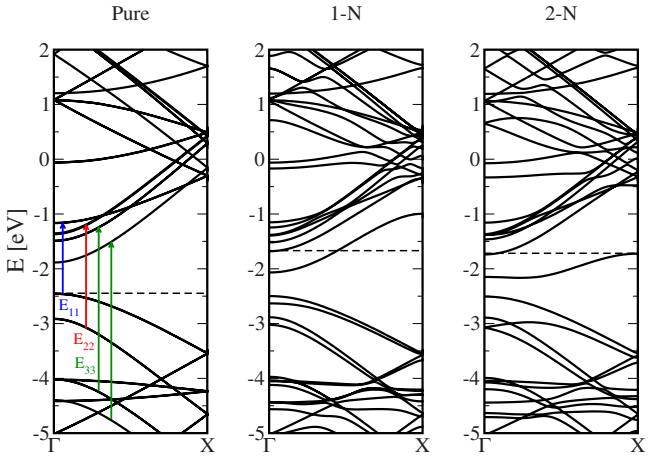

FIG. 5. (Color online) Electronic band structures of pure, 1-N doped and 2-N doped (**C** configuration) nanotubes. First optical transitions of pristine (8,0) nanotube are also given. Fermi levels are also given in dashed lines.

Experimentally, the lowest transition with respect to the optical transition selection rules is detected in photoluminescence excitation spectroscopy after absorption to higher optical transitions. Photoluminescence spectroscopy is limited to semiconducting tubes whereas resonant Raman spectroscopy applies to metallic and semiconducting tubes allowing to study the transition E_{11}, E_{22}, or E_{33} for all tubes. The photoluminescence intensity for zigzag tubes is close to zero[12] and increases with chiral angle to be maximum for armchair tubes.

Resonant Raman spectroscopy of RBMs can be performed at different singularities in the joined density of states corresponding to the transition E_{11} and E_{22} with empty conduction bands. The splitting of the conduction bands for E_{11} or E_{22} transitions is associated to the splitting of the valence bands. The transition energy E_{11} increases by 0.05 eV, while the transition energy E_{22} decreases slightly by 0.09 eV with doping. These shifts in the transition energies are comparable of the width of the Raman resonance profile of individual tubes. Clearly, doping is expected to influence the resonance profile but does not change the resonance condition drastically.

V. CONCLUSION

We have studied the influence of nitrogen doping in (8,0) CNTs on the RBM using DFT calculations including the full-potential PAW framework and frozen phonon approach. The results are compared with a one-dimensional spring constant model. Considering several doping configurations, we find that the downshift of the RBM band depends on the exact position of the dopant within the tube wall. The formation of N-N bonds is not favored for zigzag tubes. Symmetric position of the dopant leads to only small downshifts of RBM frequencies. The one-dimensional spring constant model predicts similar frequency downshifts but, due to its simplicity, different doping configurations cannot be discriminated. Electronic structure calculations show that the resonant Raman profile is expected to be shifted less than 0.1 eV when doping or creating defects.

ACKNOWLEDGMENTS

The authors would like to thank R. Poteau (Toulouse) for numerous fruitful discussions. Grants of computer time from CICT-CALMIP in Toulouse are gratefully acknowledged.

*igerber@insa-toulouse.fr
†Present address: El-Manar Preparatory Institute for Engineers Studies, Tunis-El Manar University, Tunisia.

[1] R. Saito, G. Dresslhaus, and M. S. Dresselhaus, *Physical Properties of Carbon Nanotubes* (Imperial College, London, 1999).
[2] B. Kitiyanan, W. E. Alvarez, J. H. Harwell, and D. E. Resasco, Chem. Phys. Lett. **317**, 497 (2000).
[3] J.-Y. Yi and J. Bernholc, Phys. Rev. B **47**, 1708 (1993).
[4] H. J. Choi, J. Ihm, S. G. Louie, and M. L. Cohen, Phys. Rev. Lett. **84**, 2917 (2000).
[5] R. Czerw *et al.*, Nano Lett. **1**, 457 (2001).
[6] M. Terrones *et al.*, Appl. Phys. A: Mater. Sci. Process. **74**, 355 (2002).
[7] A. H. Nevidomskyy, G. Csányi, and M. C. Payne, Phys. Rev. Lett. **91**, 105502 (2003).
[8] M. S. Dresselhaus, G. Dresselhaus, and P. C. Ecklund, *Science of Fullerenes and Carbon Nanotubes* (Academic, New York, 1996).
[9] R. A. Jishi, L. Venkataraman, M. S. Dresselhaus, and G. Dresselhaus, Chem. Phys. Lett. **209**, 77 (1993).
[10] J. Kürti, G. Kresse, and H. Kuzmany, Phys. Rev. B **58**, R8869 (1998).
[11] A. Jorio, R. Saito, J. H. Hafner, C. M. Lieber, M. Hunter, T. McClure, G. Dresselhaus, and M. S. Dresselhaus, Phys. Rev. Lett. **86**, 1118 (2001).
[12] S. M. Bachilo, M. S. Strano, C. Kittrell, R. H. Hauge, R. E. Smalley, and R. B. Weisman, Science **298**, 2361 (2002).
[13] C. Kramberger, R. Pfeiffer, H. Kuzmany, V. Zólyomi, and J. Kürti, Phys. Rev. B **68**, 235404 (2003).
[14] H. Telg, J. Maultzsch, S. Reich, F. Hennrich, and C. Thomsen, Phys. Rev. Lett. **93**, 177401 (2004).
[15] A. Jorio *et al.*, Phys. Rev. B **71**, 075401 (2005).
[16] Z. Chen, J. Zhao, T. Yano, and T. Ooie, Appl. Phys. A: Mater. Sci. Process. **74**, 213 (2002).
[17] G. D. Mahan, Phys. Rev. B **65**, 235402 (2002).
[18] J. Kürti, V. Zólyomi, M. Kertesz, and G. Sun, New J. Phys. **5**, 125 (2003).
[19] H. M. Lawler, D. Areshkin, J. W. Mintmire, and C. T. White, Phys. Rev. B **72**, 233403 (2005).
[20] R. Krupke, F. Hennrich, H. v. Lohneysen, and M. M. Kappes, Science **301**, 344 (2003).
[21] S. B. Fagan, A. S. Filho, J. M. Filho, P. Corio, and M. Dresselhaus, Chem. Phys. Lett. **406**, 54 (2005).
[22] P. Corio, A. Jorio, N. Demir, and M. Dresselhaus, Chem. Phys.

Lett. **392**, 396 (2004).
[23] G. Kresse and J. Furthmüller, Comput. Mater. Sci. **6**, 15 (1996).
[24] G. Kresse and J. Furthmüller, Phys. Rev. B **54**, 11169 (1996).
[25] P. E. Blöchl, Phys. Rev. B **50**, 17953 (1994).
[26] G. Kresse and D. Joubert, Phys. Rev. B **59**, 1758 (1999).
[27] J. P. Perdew, K. Burke, and M. Ernzerhof, Phys. Rev. Lett. **77**, 3865 (1996); **78**, 1396(E) (1997).
[28] J. Maultzsch, H. Telg, S. Reich, and C. Thomsen, Phys. Rev. B **72**, 205438 (2005).
[29] C. Fantini, A. Jorio, M. Souza, M. S. Strano, M. S. Dresselhaus, and M. A. Pimenta, Phys. Rev. Lett. **93**, 147406 (2004).
[30] J. C. Meyer, M. Paillet, T. Michel, A. Moréac, A. Neumann, G. S. Duesberg, S. Roth, and J.-L. Sauvajol, Phys. Rev. Lett. **95**, 217401 (2005).
[31] A. Hashimoto, K. Suenaga, A. Gloter, K. Urita, and S. Iijima, Nature (London) **430**, 870 (2004).
[32] L. G. Bulusheva, A. V. Okotrub, A. G. Kudashov, A. P. Asanov, and O. G. Abrosimov, Eur. Phys. J. D **34**, 271 (2005).
[33] F. Xu, M. Minniti, C. Giallombardo, A. Cupolillo, P. Barone, A. Oliva, and L. Papagno, Surf. Sci. **601**, 2819 (2007).
[34] H. S. Kang and S. Jeong, Phys. Rev. B **70**, 233411 (2004).
[35] S. H. Lim, R. Li, W. Ji, and J. Lin, Phys. Rev. B **76**, 195406 (2007).
[36] S. S. Yu, Q. B. Wen, W. T. Zheng, and Q. Jiang, Nanotechnology **18**, 165702 (2007).
[37] S. H. Yang, W. H. Shin, and J. K. Kang, Small **4**, 437 (2008).
[38] S. Niyogi, M. Hamon, H. Hu, B. Zhao, P. Bhowmik, R. Sen, M. Itkis, and R. Haddon, Acc. Chem. Res. **35**, 1105 (2002).
[39] Y.-H. Kim, J. Choi, K. J. Chang, and D. Tománek, Phys. Rev. B **68**, 125420 (2003).
[40] P. O. Lehtinen, A. S. Foster, Y. Ma, A. V. Krasheninnikov, and R. M. Nieminen, Phys. Rev. Lett. **93**, 187202 (2004).
[41] A. J. Lu and B. C. Pan, Phys. Rev. Lett. **92**, 105504 (2004).
[42] S. Berber and A. Oshiyama, Physica B **376-377**, 272 (2006).
[43] M. Terrones *et al.*, Adv. Mater. (Weinheim, Ger.) **11**, 655 (1999).
[44] M. Zhao, Y. Xia, J. P. Lewis, and R. Zhang, J. Appl. Phys. **94**, 2398 (2003).
[45] R. A. Jishi, M. S. Dresselhaus, and G. Dresselhaus, Phys. Rev. B **48**, 11385 (1993).
[46] D. Sánchez-Portal, E. Artacho, J. M. Soler, A. Rubio, and P. Ordejón, Phys. Rev. B **59**, 12678 (1999).
[47] J. X. Cao, X. H. Yan, Y. Xiao, Y. Tang, and J. W. Ding, Phys. Rev. B **67**, 045413 (2003).
[48] E. Dobardžić, I. Milošević, B. Nikolić, T. Vuković, and M. Damnjanovic, Phys. Rev. B **68**, 045408 (2003).
[49] M. Machón, S. Reich, H. Telg, J. Maultzsch, P. Ordejón, and C. Thomsen, Phys. Rev. B **71**, 035416 (2005).
[50] Y. Xiao, Z. M. Li, X. H. Yan, Y. Zhang, Y. L. Mao, and Y. R. Yang, Phys. Rev. B **71**, 233405 (2005).
[51] J. Zimmermann, P. Pavone, and G. Cuniberti, Phys. Rev. B **78**, 045410 (2008).
[52] D. Gunlycke, H. M. Lawler, and C. T. White, Phys. Rev. B **77**, 014303 (2008).
[53] B. K. Agrawal, S. Agrawal, and R. Srivastava, J. Phys.: Condens. Matter **16**, 1467 (2004).
[54] Z. X. Guo, J. W. Ding, Y. Xiao, and D. Y. Xing, Nanotechnology **18**, 465706 (2007).
[55] H. Y. He and B. C. Pan, Phys. Rev. B **77**, 073410 (2008).
[56] C. D. Spataru, S. Ismail-Beigi, L. X. Benedict, and S. G. Louie, Phys. Rev. Lett. **92**, 077402 (2004).